Current Biology

Supplemental Information

Complete Genomes Reveal Signatures of Demographic and Genetic Declines in the Woolly Mammoth

Eleftheria Palkopoulou, Swapan Mallick, Pontus Skoglund, Jacob Enk, Nadin Rohland, Heng Li, Ayça Omrak, Sergey Vartanyan, Hendrik Poinar, Anders Götherström, David Reich, and Love Dalén

Supplemental Figures

A Wrangel library

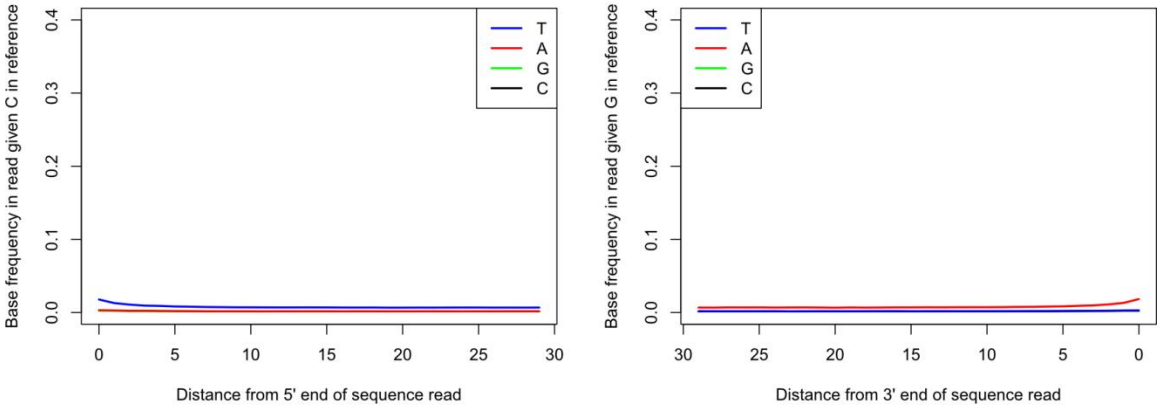

B Oimyakon library

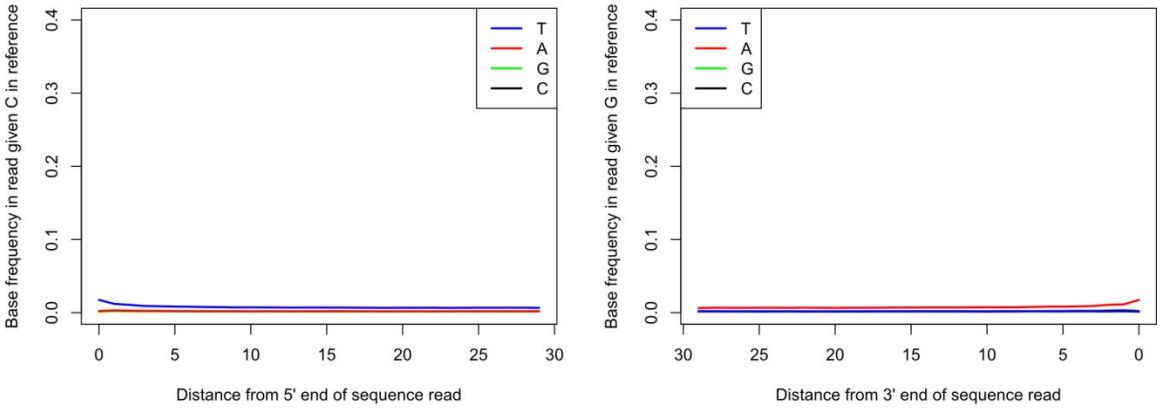

C P875_505 library

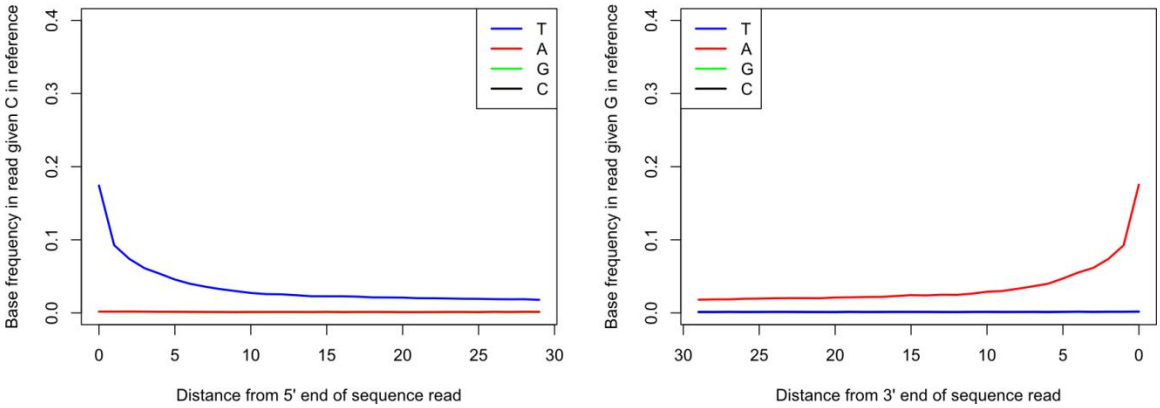

D Wrangel mtDNA reads

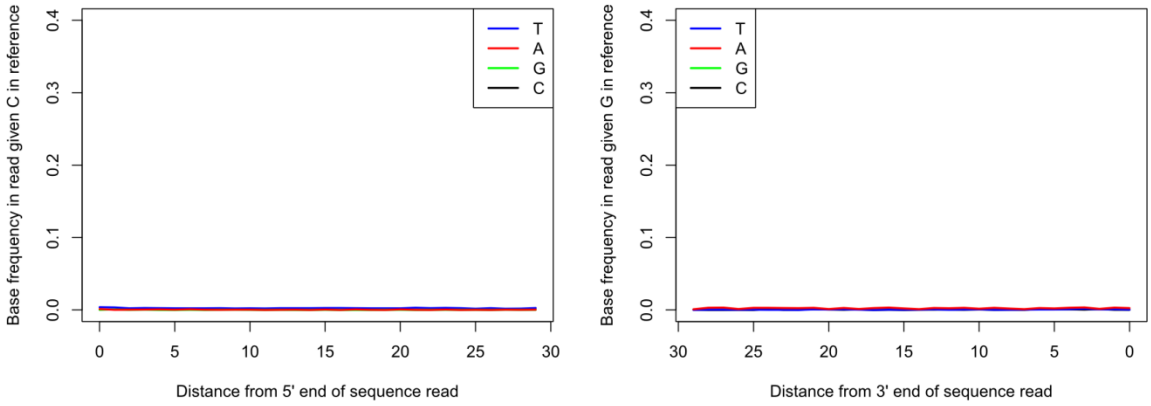

E Oimyakon mtDNA reads

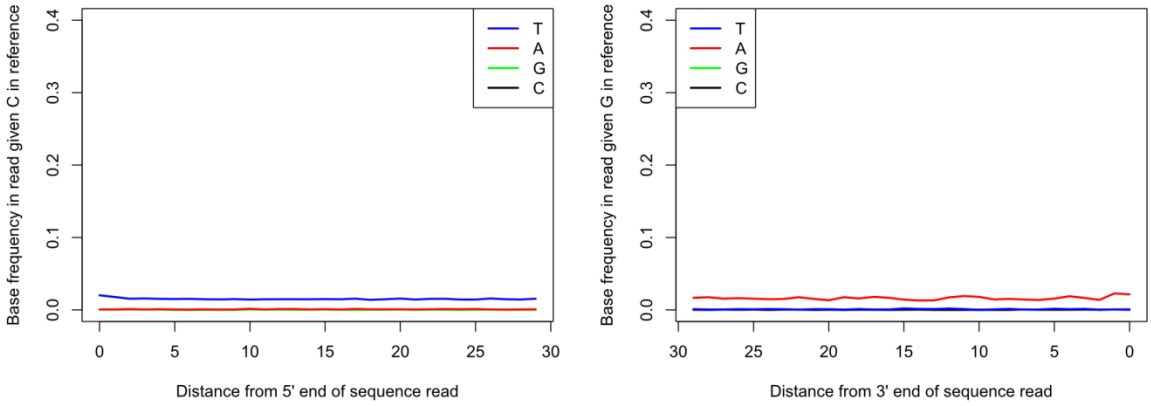

F Wrangel CpG reads

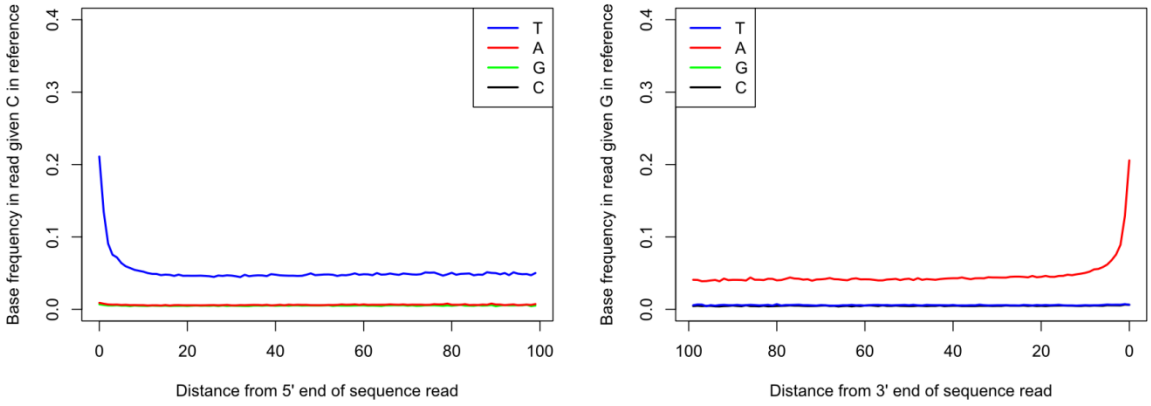

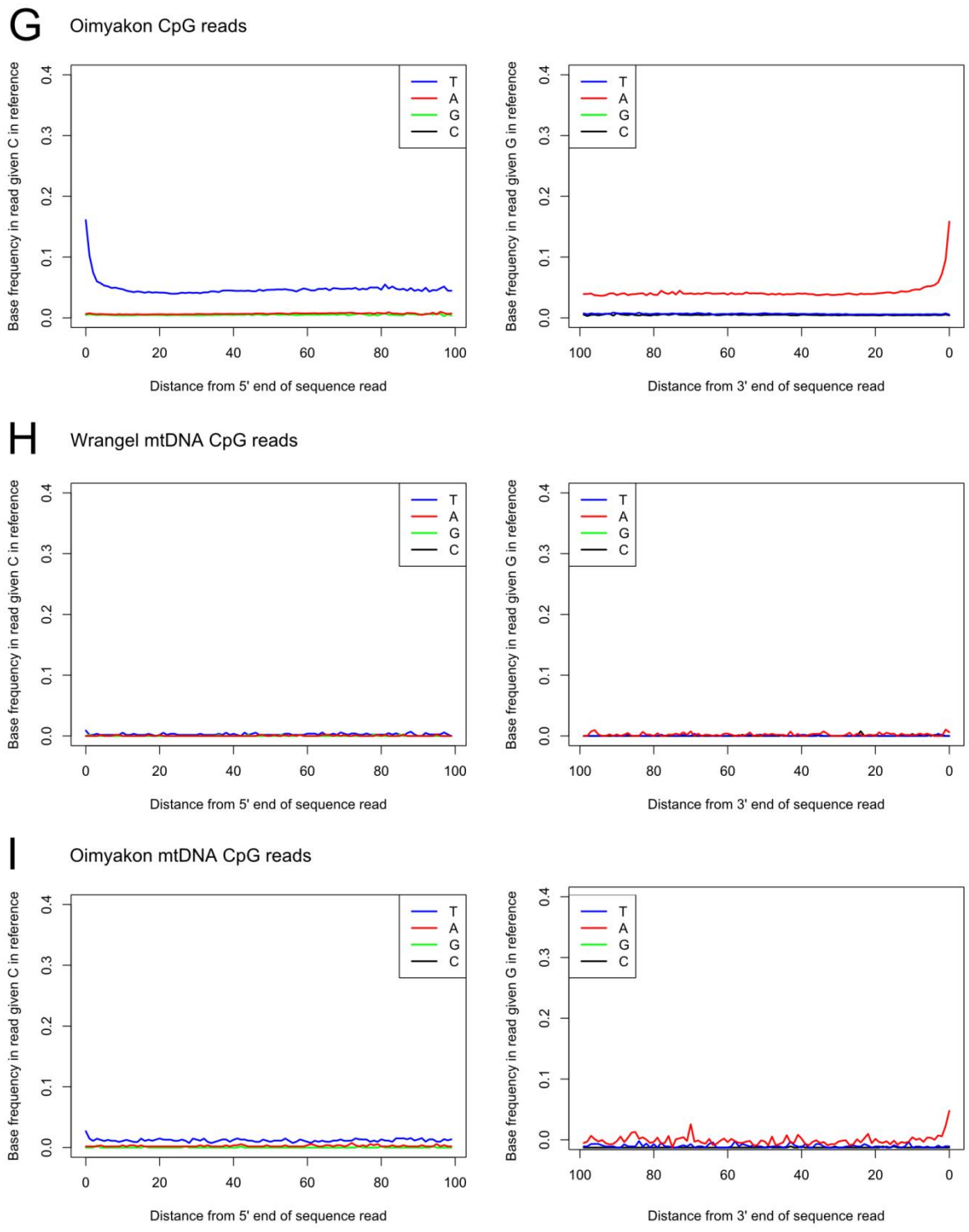

Figure S1. Nucleotide misincorporation patterns of the woolly mammoth DNA libraries. (A-B) Damage-derived substitutions in the Wrangel and Oimyakon UDG-treated libraries. (C) Damage-derived substitutions in the non-UDG treated library P875_505.

(D-E) Damage-derived substitutions in the mtDNA reads of the UDG-treated libraries. (F-G) Damage-derived substitutions in reads with CpG dinucleotides from the UDG-treated libraries. (H-I) Damage-derived susbsitutions in mtDNA reads with CpG dinucleotides from the UDG-treated libraries.

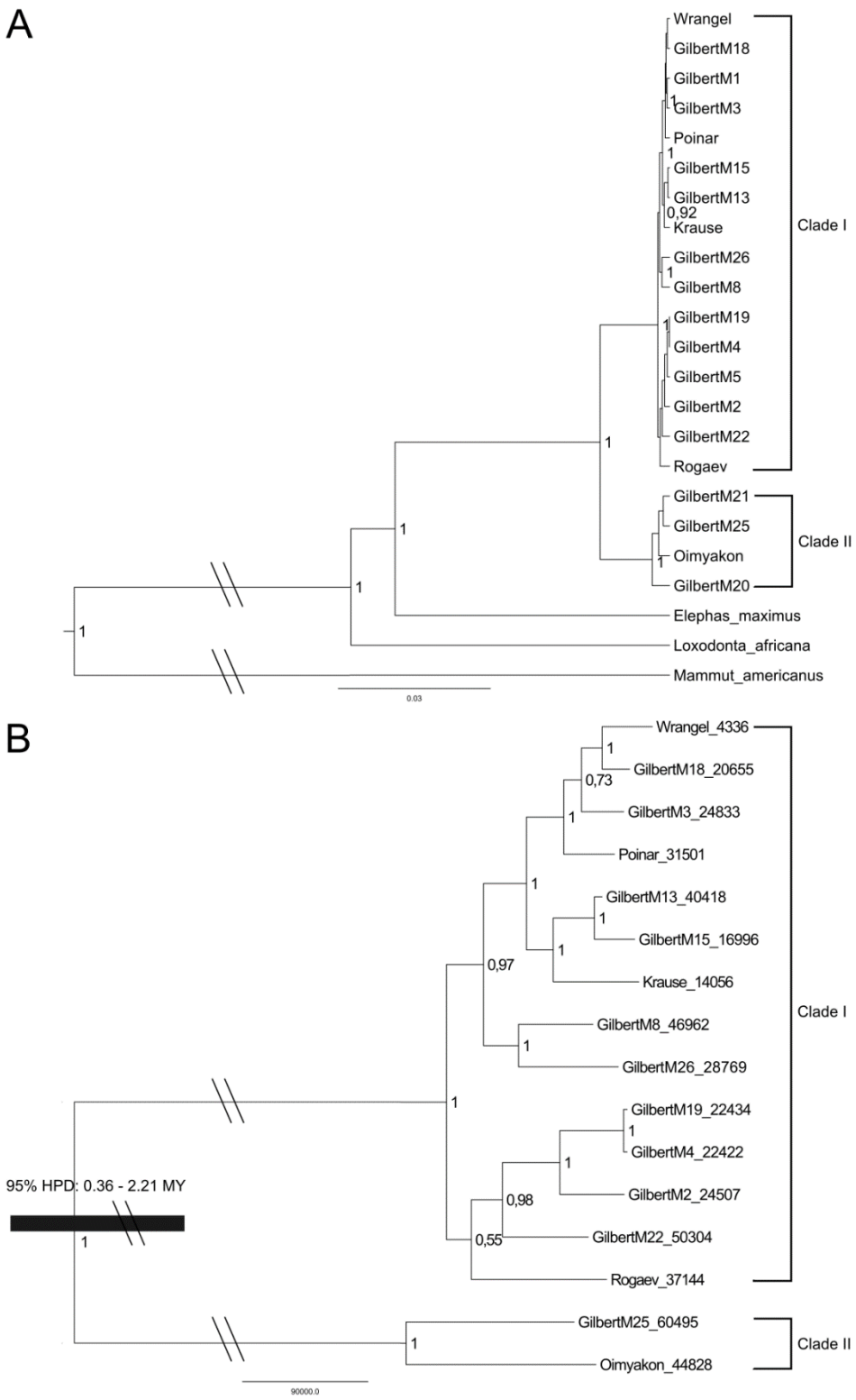

Figure S2. Mitochondrial DNA clade membership of the two woolly mammoths.

(A) Bayesian phylogeny of complete mt genomes from 20 woolly mammoths, an Asian elephant, an African savanna elephant and a mastodon. (B) Dated phylogeny of complete mt genomes from 16 woolly mammoths with finite radiocarbon dates. The median calibrated date of each mitochondrial genome sequence is shown next to the tip label. The black bar represents the 95% highest posterior density of the nodal age estimate. Bayesian posterior probabilities are shown. Branches with crossed lines on them indicate that they have been shortened for illustrative purposes. Mitochondrial DNA clades I and II are indicated.

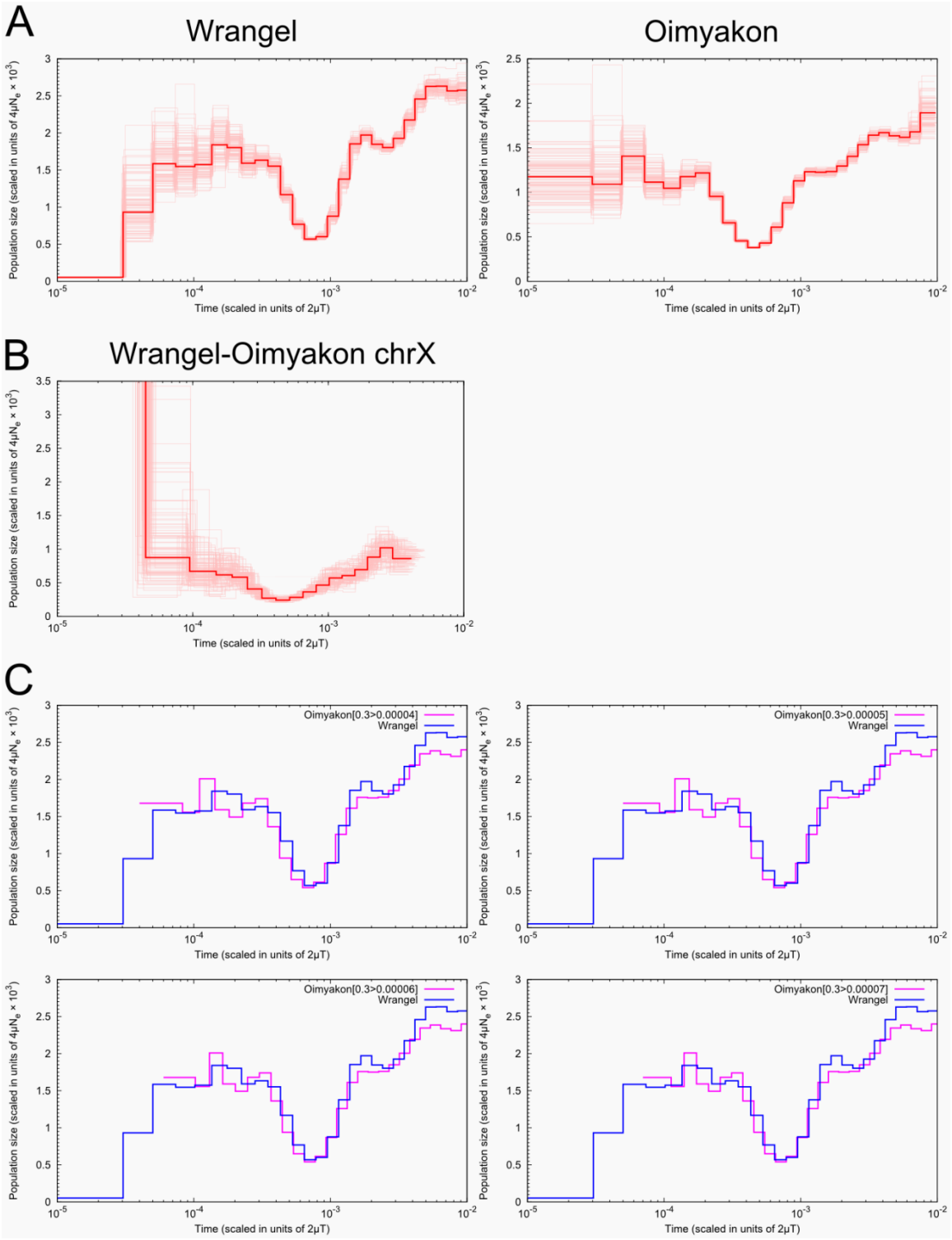
A
Wrangel
Oimyakon
B
Wrangel-Oimyakon chrX
C
Oimyakon[0.3>0.00004]
Oimyakon[0.3>0.00005]
Oimyakon[0.3>0.00006]
Oimyakon[0.3>0.00007]
Wrangel
Population size (scaled in units of 4μN_e × 10^3)
Time (scaled in units of 2μT)

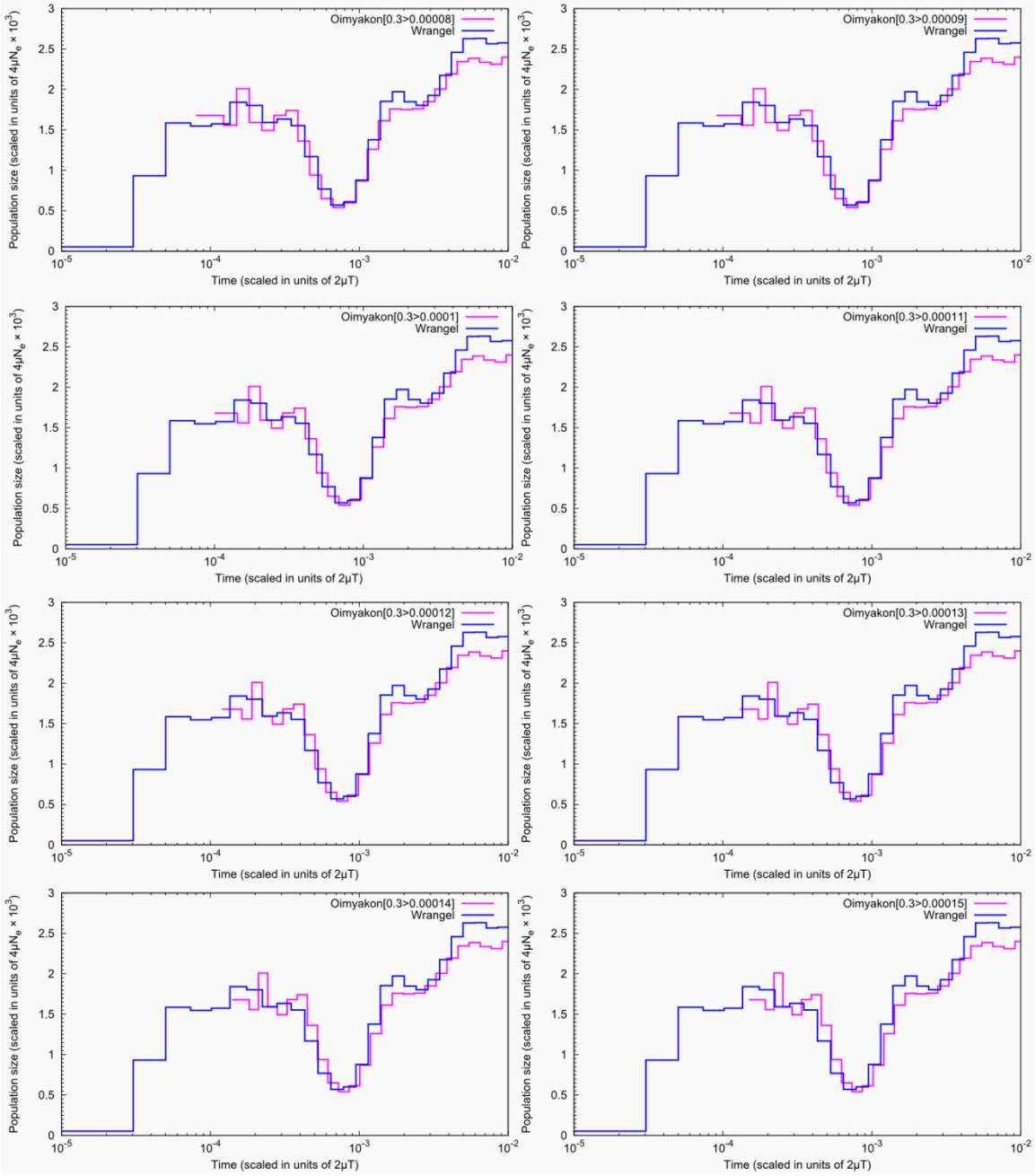

Figure S3. PSMC estimates of the Wrangel genome, Oimyakon genome and Wrangel-Oimyakon chromosome X. Time on the lower x-axis is given in units of divergence per base pair. Population size on the y-axis is given in units of $4\mu N_e \times 10^3$. (A) Thick red lines represent the PSMC estimate of each genome and thin red lines represent

the curves from 100 rounds of bootstrap analyses. (B) The thick red line represents the PSMC estimate of the Wrangel-Oimyakon pseudo-diploid chromosome X and the thin red lines represent the curves from 100 rounds of bootstrap analyses. (C) PSMC estimates of the two genomes plotted together with the Oimyakon curve shifted along the x-axis until its population history was lined up with that of the Wrangel genome (d= 0.00004 – 0.00015). An empirical false negative rate of 30% was applied on the Oimyakon curve to correct for missing heterozygotes due to its lower coverage.

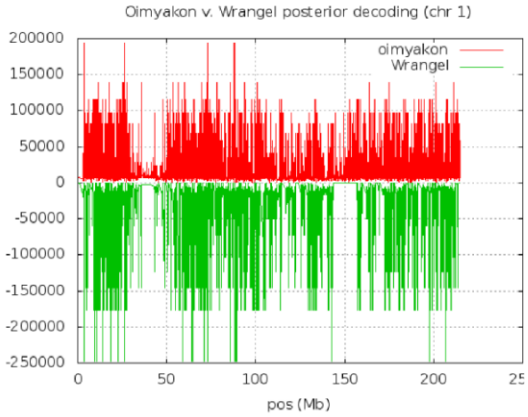
Oimyakon v. Wrangel posterior decoding (chr 1)
oimyakon
Wrangel
pos (Mb)

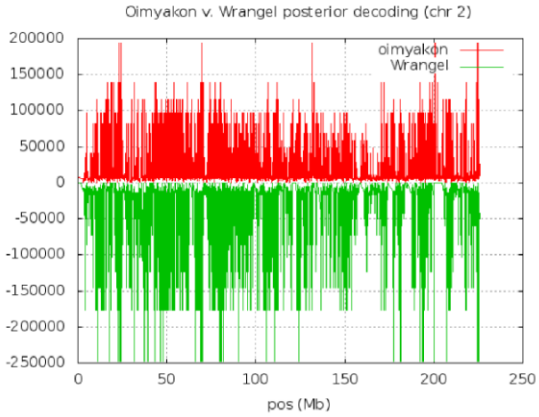
Oimyakon v. Wrangel posterior decoding (chr 2)
oimyakon
Wrangel
pos (Mb)

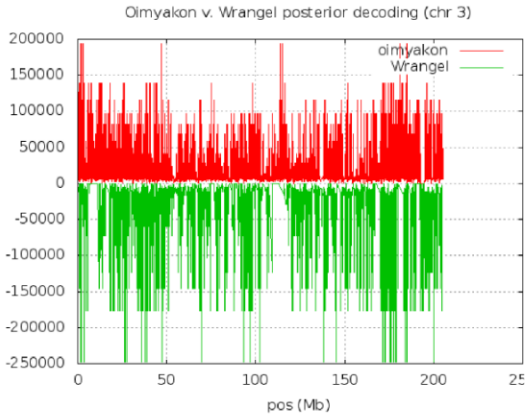
Oimyakon v. Wrangel posterior decoding (chr 3)
oimyakon
Wrangel
pos (Mb)

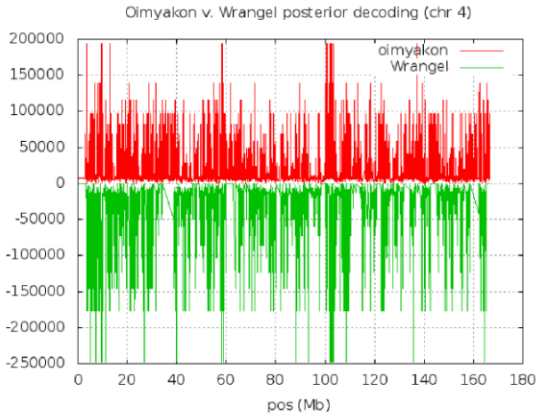
Oimyakon v. Wrangel posterior decoding (chr 4)
oimyakon
Wrangel
pos (Mb)

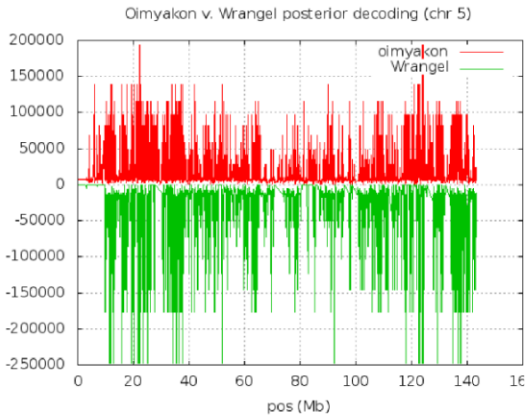
Oimyakon v. Wrangel posterior decoding (chr 5)
oimyakon
Wrangel
pos (Mb)

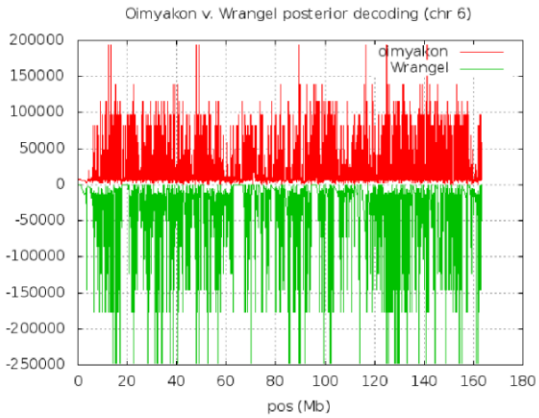
Oimyakon v. Wrangel posterior decoding (chr 6)
oimyakon
Wrangel
pos (Mb)

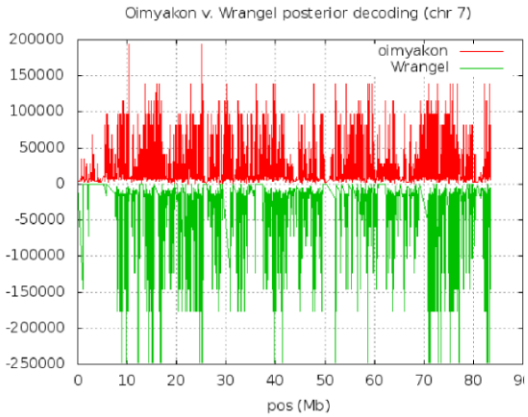
Oimyakon v. Wrangel posterior decoding (chr 7)
oimyakon
Wrangel
pos (Mb)

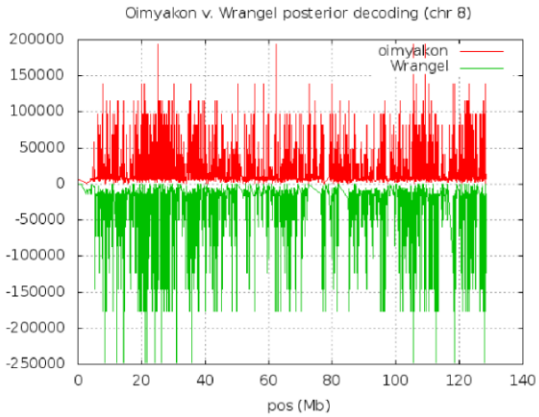
Oimyakon v. Wrangel posterior decoding (chr 8)
oimyakon
Wrangel
pos (Mb)

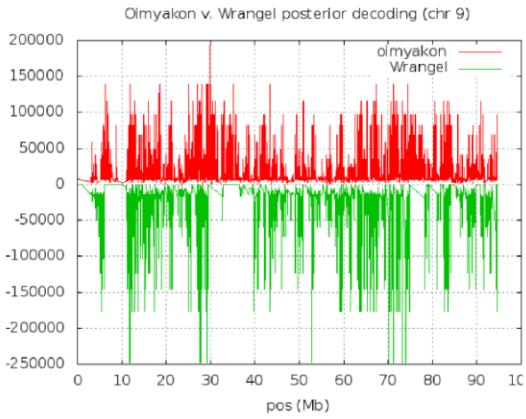
Oimyakon v. Wrangel posterior decoding (chr 9)
oimyakon
Wrangel
pos (Mb)

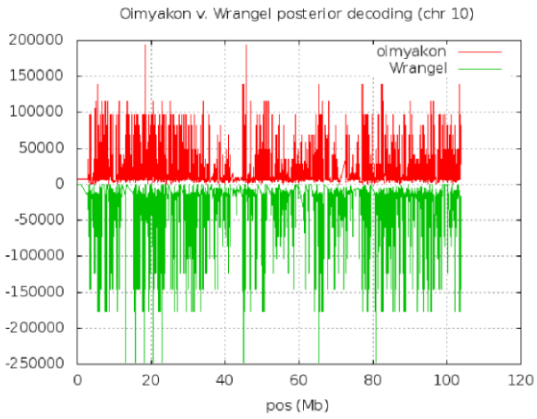
Oimyakon v. Wrangel posterior decoding (chr 10)
oimyakon
Wrangel
pos (Mb)

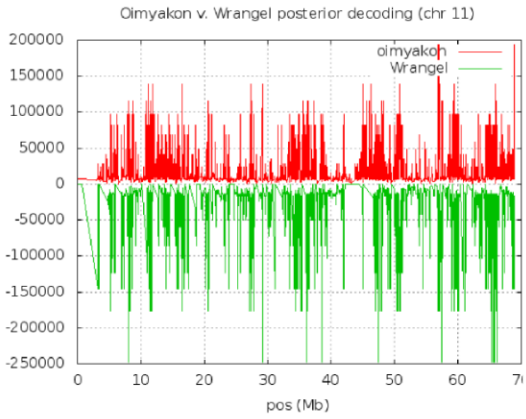
Oimyakon v. Wrangel posterior decoding (chr 11)
oimyakon
Wrangel
pos (Mb)

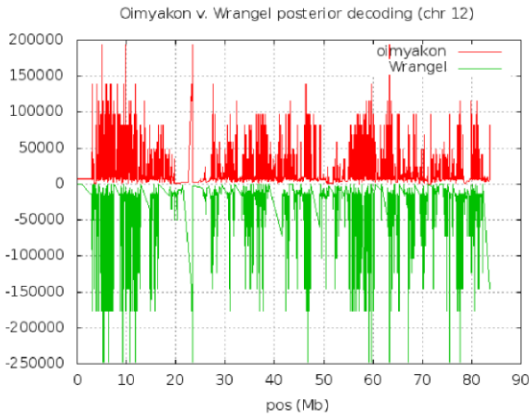
Oimyakon v. Wrangel posterior decoding (chr 12)
oimyakon
Wrangel
pos (Mb)

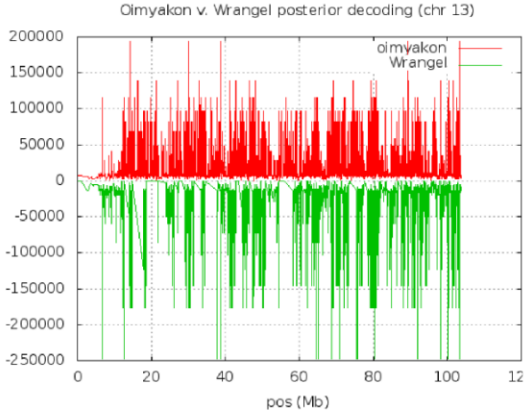
Oimyakon v. Wrangel posterior decoding (chr 13)
oimyakon
Wrangel
pos (Mb)

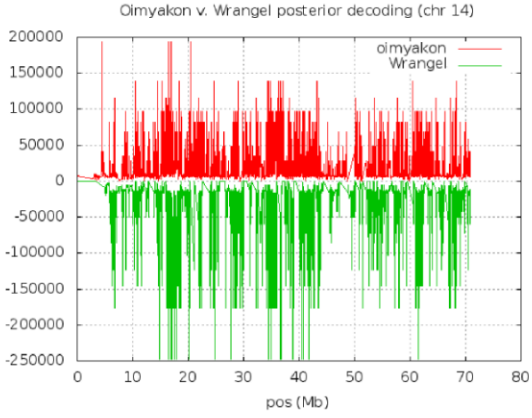
Oimyakon v. Wrangel posterior decoding (chr 14)
oimyakon
Wrangel
pos (Mb)

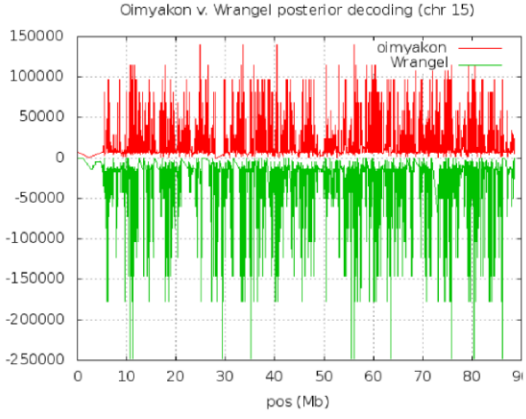
Oimyakon v. Wrangel posterior decoding (chr 15)
oimyakon
Wrangel
pos (Mb)

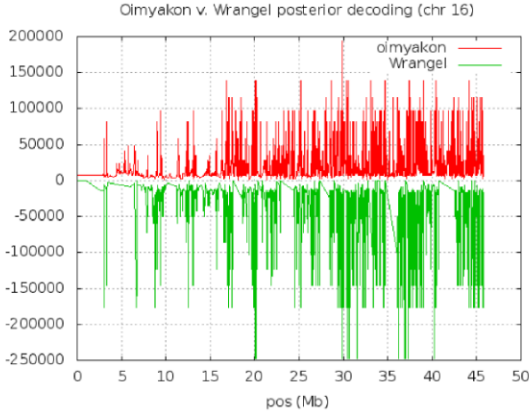
Oimyakon v. Wrangel posterior decoding (chr 16)
oimyakon
Wrangel
pos (Mb)

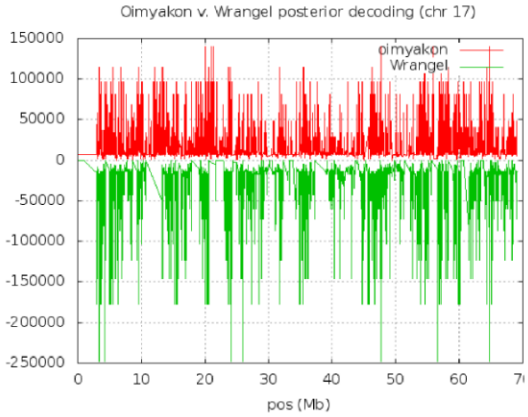
Oimyakon v. Wrangel posterior decoding (chr 17)
oimyakon
Wrangel
pos (Mb)

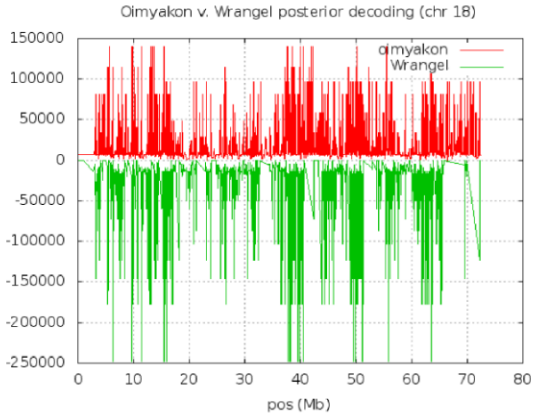
Oimyakon v. Wrangel posterior decoding (chr 18)
oimyakon
Wrangel
pos (Mb)

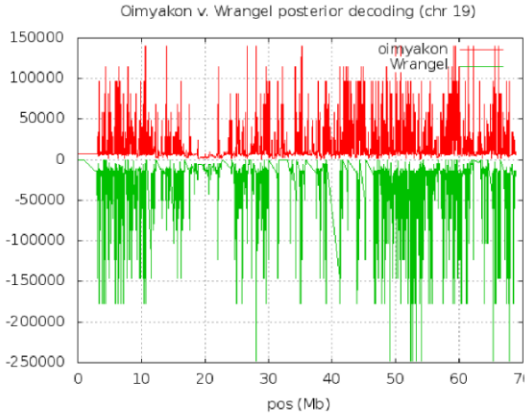
Oimyakon v. Wrangel posterior decoding (chr 19)
oimyakon
Wrangel
pos (Mb)

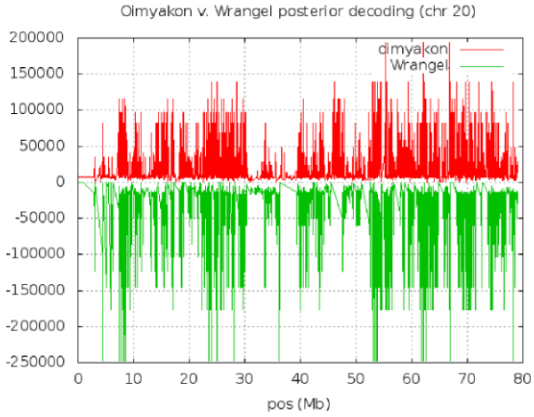
Oimyakon v. Wrangel posterior decoding (chr 20)
oimyakon
Wrangel
pos (Mb)

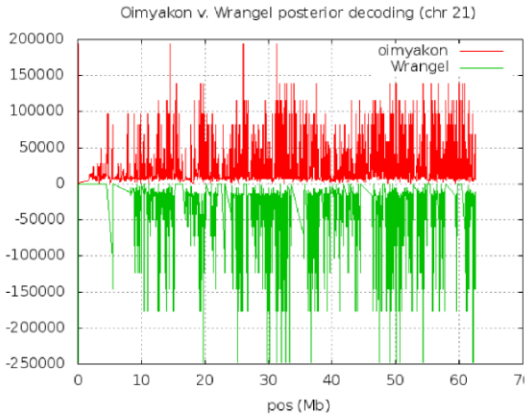
Oimyakon v. Wrangel posterior decoding (chr 21)
oimyakon
Wrangel
pos (Mb)

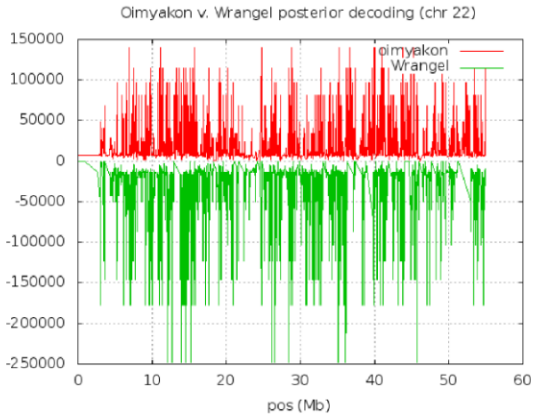
Oimyakon v. Wrangel posterior decoding (chr 22)
oimyakon
Wrangel
pos (Mb)

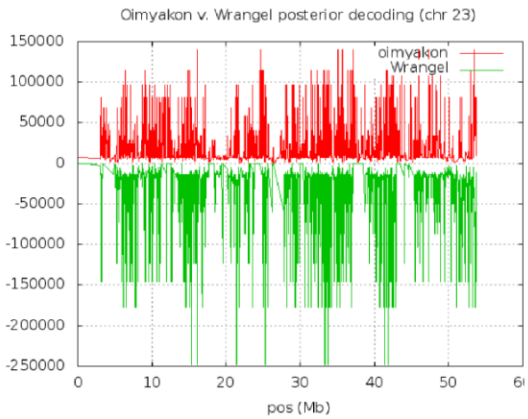
Oimyakon v. Wrangel posterior decoding (chr 23)
oimyakon
Wrangel
pos (Mb)

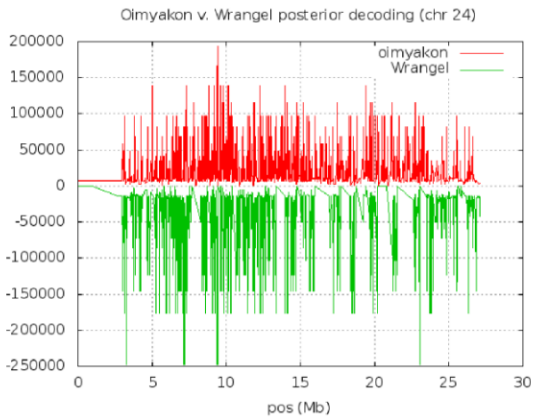
Oimyakon v. Wrangel posterior decoding (chr 24)
oimyakon
Wrangel
pos (Mb)

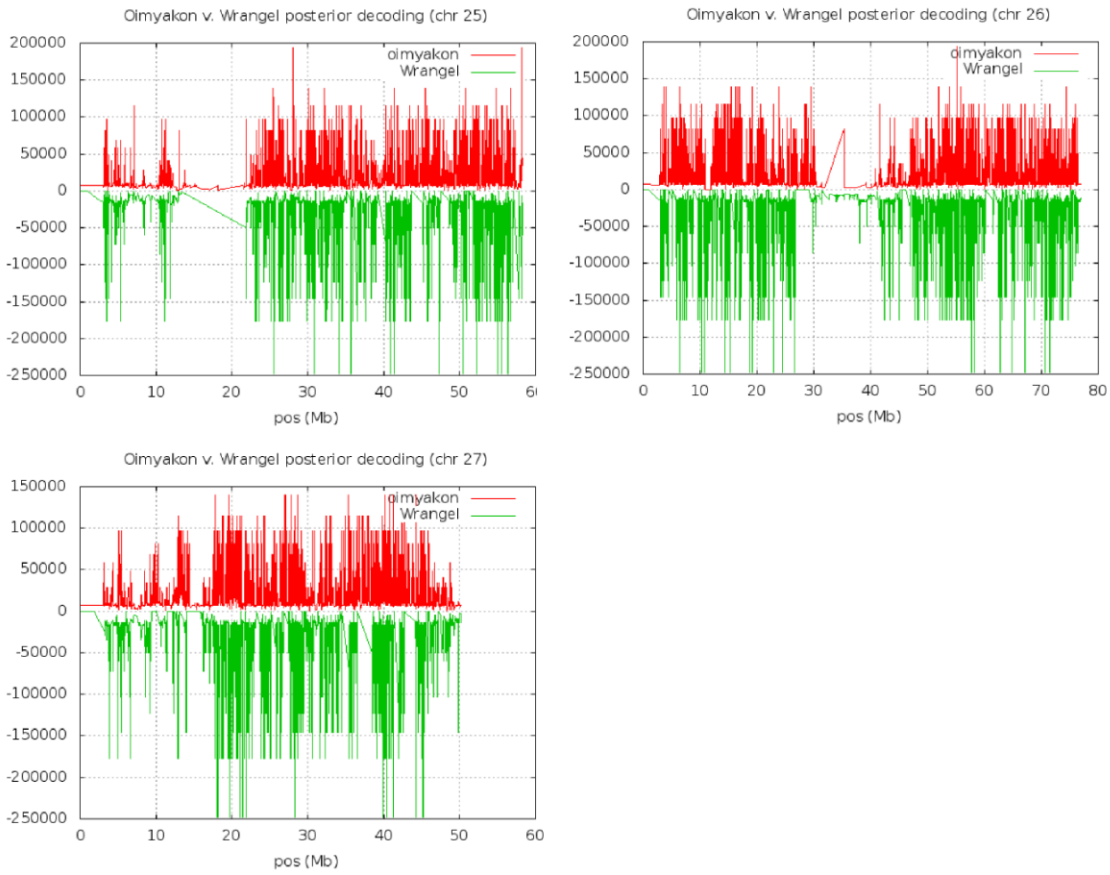

Figure S4. Distribution of the inferred TMRCA for the two alleles of chromosomes 1-27 of each individual. The Oimyakon individual is shown in red and the Wrangel individual in green.

Table S1: Specimen information and summary of data from individuals from Wrangel Island that were pooled for shotgun-sequencing.

Extraction No	^{14}C age	Material	# raw reads ($\times 10^6$)	% mapped	% clonal	Total mapped reads
E460B	4400±40	Tusk	6.85	80.91	1.31	5469674
E461B	4389±46	Bone	6.14	39.12	1.58	2363681
E462B	4370±40	Tusk	13.07	0.35	0.20	45564
E463B	4260±75	Molar	5.27	8.11	0.84	423965
E464B	4210±70	Molar	16.48	68.11	1.82	11020619
E465B	4120±110	Tusk	4.77	10.68	1.17	503660
E466B	3920±40	Tusk	5.58	18.27	0.85	1011026
E467B	3905±47	Molar	9.61	77.45	1.70	7317141
E468B	3730±40	Tusk	6.34	16.95	0.64	1067848
E469B	3685±60	Molar	5.19	17.54	1.45	897036
E460C	4400±40	Tusk	5.77	86.47	1.96	4891320
E461C	4389±46	Bone	5.61	13.65	0.87	758942
E462C	4370±40	Tusk	6.17	0.57	0.26	34970
E463C	4260±75	Molar	4.86	8.76	0.85	422129
E464C	4210±70	Molar	5.31	72.44	1.32	3796066
E465C	4120±110	Tusk	3.87	13.76	16.56	444308
E467C	3905±47	Molar	6.81	80.51	1.37	5407532
E468C	3730±40	Tusk	6.34	16.51	5.01	994459

Extraction numbers B and C refer to two different DNA isolation protocols that were used for each specimen (see Supplemental Experimental Procedures).

Table S2: Heterozygosity estimates per 1,000 base pairs.

	mlRho autosomes				mlRho chrX			
	θ	CI (θ)	ε	CI (ε)	θ	CI (θ)	ε	CI (ε)
Wrangel	1.00	0.99-1.02	0.504	0.501-0.508	0.439	0.272-0.661	0.357	0.296-0.426
Oimyakon	1.25	1.23-1.27	0.558	0.554-0.563	0.225	0.088-0.457	0.296	0.217-0.391

(θ): population mutation rate which approximates heterozygosity under the infinite sites model.

(ε) : sequencing error estimated by mlRho.

CI: confidence interval.

Supplemental Experimental Procedures

Sample description, radiocarbon dating

The Wrangel specimen is a molar collected by one of us (Sergey Vartanyan) on Wrangel Island (70°-72° N and 178°-177° W; Figure 1A). Radiocarbon dating at the University of Arizona (Tucson, USA) using accelerator mass spectrometry (AMS) had previously produced an uncalibrated age of 3,905± 47 radiocarbon years [S1] (AA 40665). This specimen has already been characterized for 741bp of mitochondrial DNA including part of the cytochrome b gene (CytB), two tRNA genes (tRNA-Thr and tRNA-Pro) and the first hypervariable part of the control region (CR1) [S2] as well as for four microsatellite markers [S3].

The Oimyakon specimen is soft tissue (skin) from the remains of a woolly mammoth calf found in the Oimyakon district, Yakutia (63.50° N 142.75° W; Figure 1A) [S4]. This specimen was collected from the Cerpolex/Mammuthus collection in Khatanga, Russia. Skin from the remains of the calf was dated with AMS to an uncalibrated age of 41,300± 900 radiocarbon years BP [S4] (GrA-30727). This specimen has already been characterized for 743bp of mitochondrial DNA including part of the cytochrome b gene (CytB), two tRNA genes (tRNA-Thr and tRNA-Pro) and the first hypervariable part of the control region (CR1) [S5].

Both radiocarbon dates were calibrated in OXCAL [S6] v. 4.2 with the IntCal 13 calibration curve [S7]. The median calibrated date corresponds to 4,336 (99.7% posterior range: 4,147 – 4,523) years for the Wrangel specimen and 44,828 (99.7% posterior range: 42,753 – 48,045) years for the Oimyakon specimen (Figure 1B).

DNA extraction, library preparation and sequencing

Wrangel specimen

In an initial screening experiment we performed shotgun-sequencing of ten individuals with the most recent radiocarbon dates from our sample collection from Wrangel Island to determine their level of endogenous DNA (Table S1). We generated two DNA extracts from each specimen following two methods and using 50 mg of bone powder for each extraction method: *i)* a modified version of protocol C in Yang *et al.* [S8] as described in Brace *et al.* [S9] (extraction numbers B in Table S1) and *ii)* protocol C in [S10] (extraction numbers C in Table S1) with the following modifications: PB buffer (Qiagen) was used as binding buffer instead of L2 and EB (Qiagen) was used to elute DNA instead of 1X TE buffer. A 362bp fragment of the mitochondrial DNA was amplified using primers mam_15038F and mam_15401R [S11] to assess successful DNA yield. Negative controls were always included in extraction and amplification sets. All specimens amplified successfully for the targeted DNA region with the first extraction method while two specimens failed to yield amplifiable DNA with the second extraction method. We prepared indexed double-stranded libraries from the positive DNA extracts including water controls and following the protocol for multiplexed sequencing by Meyer & Kircher [S12], using AmpliTaq Gold® (Life technologies) for the indexing PCR. Indexed libraries were purified with magnetic beads (Agencourt AMPure XP, Beckman Coulter) and their concentration was measured using a high-sensitivity DNA chip on the Bioanalyzer 2100 (Agilent). Finally, all indexed libraries were pooled in equimolar concentrations and sequenced in one lane of an Illumina HiSeq 2500 flowcell with a paired-end 2x100bp setup in RapidRun mode.

We processed reads as described in the following section (sequence processing and alignment) and estimated the percentage of reads that aligned to the African elephant reference genome and the percentage of clonal reads for each library. Table S1 shows that libraries built from each of the two extracts from the same specimen yielded similar levels of endogenous DNA (no significant differences according to pairwise t-tests for percentage of mapped reads depending on extraction protocol, $P = 0.38$). Three specimens contained fractions of endogenous DNA higher than 50% with low percentage of clonal reads and the specimen with the youngest date (E467) was chosen for deeper whole genome sequencing.

We prepared a new library from 20ul of the E467C DNA extract using the same double-stranded library protocol [S12] as the one used for the screening experiment described above. Treatment with the USER enzyme (New England Biolabs) was performed during blunt-end repair to excise uracil residues [S13, S14] and a high-fidelity polymerase AccuPrime™ Pfx (Life technologies) was used for the indexing PCR. Six independent amplifications were performed for indexing (using six different indexes as suggested by Meyer & Kircher [S12] to avoid a downstream failure of Illumina's image analysis software), which were then pooled. Purification of the pooled library was performed with magnetic beads (Agencourt AMPure XP, Beckman Coulter) and its concentration was measured using a high-sensitivity DNA chip on the Bioanalyzer 2100 (Agilent). Sequencing was performed on 8 lanes of the Illumina HiSeq 2500 flowcell with a paired-end 2x100bp setup in HighOutput mode. All pre-PCR DNA analyses described above were performed in a dedicated ancient DNA laboratory at the Swedish Museum of Natural History in Stockholm.

Oimyakon specimen

180mg of soft tissue (skin) were subsampled from the Oimyakon specimen. DNA extraction was performed following the protocol described in [S15] with some modifications: *i)* the subsample was pre-washed for 1.5h in 0.5M EDTA (pH 8.0) with agitation at room temperature, *ii)* following overnight incubation of the pellet with EDTA at room temperature, digestion was performed at 55°C for 5h, *iii)* extraction of the digested supernatant was performed using phenol:chloroform:isoamyl alcohol (PCI 25:24:1) in the first step and chloroform:isoamyl alcohol (25:1) in the second step of extraction, iv) the DNA extract was finally concentrated using a 30kDA Amicon centrifuge filter (Millipore) at 10k x g and washed four times with 0.1X TE buffer.

The DNA extract was purified using a MinElute column (QIAGEN). 20µL of the purified extract were then converted to a double-stranded, UDG-treated (with the USER enzyme mix) Illumina sequencing library [S12, S14]. The library was double-indexed using the P5 and P7 indexing primers [S14] and purified with MinElute columns (QIAGEN). Re-amplification was performed in a total of 18 reactions followed by a size-selection with gel-electrophoresis using low melting point agarose for inserts > 40bp. Excised bands were purified with the QiaQuick Gel Purification kit (QIAGEN) without applying heat during the melting of the agarose to not over-represent GC rich regions [S16]. The purified library was then re-amplified and sequenced on 7 lanes of an Illumina HiSeq 2500 platform with a paired-end 2 x 100bp single-index setup. All pre-PCR sample manipulation was performed in dedicated ancient DNA laboratory facilities at the McMaster Ancient DNA Center. DNA analyses following indexing of the DNA library

were performed at Harvard Medical School and sequencing was performed at Illumina, San Diego, USA.

Sequence processing and alignment

The reads were processed with HiSeq Control Software 2.0.12.0/RTA 1.17.21.3 and Bcl to Fastq conversion was performed using bcl2Fastq v1.8.3 from the CASAVA 1.8 software suite. Reads were sorted according to their indexes. SeqPrep 1.1 (https://github.com/jstjohn/SeqPrep) was used to remove adapters and merge paired end reads. Adapter sequences were trimmed by searching for a >= 10nt overlap between the end of each read and the adapter sequence allowing up to 0.02 mismatching bases of good quality (>13) in the overlapping region and requiring a minimum of 0.87 matching bases in the overlapping region. Forward and reverse reads were merged into single reads if they overlapped for at least 15nt allowing up to 0.02 mismatching bases of good quality (>13) and requiring a minimum of 0.9 matching bases in the overlapping region. A minor modification to the source code was performed to ensure that the quality score of bases in the merged region are the best one of the two possibilities, rather than the aggregate. Merged reads with length shorter than 30bp were discarded.

In the following steps, we used BWA [S17] version 0.7.8 and SAMtools [S18] version 0.1.19. BWA's index command was used to index the African savanna elephant (*Loxodonta africana*) genome (LoxAfr4; downloaded from ftp://ftp.broadinstitute.org/distribution/assemblies/mammals/elephant/loxAfr4/) that was used as the reference genome. Merged reads were mapped against the reference genome using parameters -l 16500 –n 0.01 –o 2, which deactivate seeding, allow more

substitutions and permit up to two gaps (instead of one), using BWA's 'aln' algorithm to construct suffix arrays. Alignments were built using BWA's 'samse' command, and converted to BAM format using SAMtools, prior to coordinate sorting. Unmapped reads were filtered out and SAMtools' 'rmdup' was used to remove duplicates with the '-s' option.

The number of aligned reads representing the fraction of endogenous DNA was equal to ~76% for the Wrangel library and ~64% for the Oimyakon library (without a mapping quality threshold). The estimated percentage of clonal reads was ~19% for Wrangel and ~30% for Oimyakon. The distribution of insert size in base pairs of the Wrangel library displays a higher average compared to the insert size of the Oimyakon library. On average, we recovered the complete genome sequence of the Wrangel individual at 17.1-fold coverage and of the Oimyakon individual at 11.2-fold coverage.

Mitochondrial genome sequence and phylogeny

We added a previously published woolly mammoth complete mitochondrial genome [S19] (GenBank accession number: DQ188829.2) to the African elephant reference genome, in order to recover both nuclear and mitochondrial (mt) DNA sequences from the two samples. Since BWA [S17] was used for alignments to the circular mt reference genome, we added 240 of the first base pairs to the end of the mt reference genome in order to facilitate mapping and avoid reduced coverage at the beginning and end of the mt genome [S20]. In total, 33,180 reads aligned to the mt genome resulting in an average 222-fold coverage for the Wrangel individual. For the Oimyakon individual, the total number of aligned reads was equal to 33,735, providing an average 299-fold coverage of

the mtDNA genome. The average length of the mtDNA reads was 150.8bp and 119.2bp for the Oimyakon and Wrangel library respectively. Both distributions were skewed towards longer read lengths compared to the length distribution of the nuclear DNA reads. We found that the difference between the length distributions of the mtDNA and nuclear reads is due to SAMtools' 'rmdup' function, which removes duplicates based on either the 5' or 3' position of the reads and retains the longest read. This leads to inflated length distribution for loci with deep coverage, such as the mitochondrion. Using an alternative script for removing duplicates based on both 5' and 3' position of the reads, and randomly retaining a read, removes the inflation effect on the length distribution of the mtDNA reads (data not shown).

We used SAMtools' [S18] (v. 0.1.19) 'mpileup' command and the 'vcf2fq' command from vcfutils.pl to generate mtDNA consensus sequences filtering out bases with quality below 30 and positions with root-mean-squared mapping quality below 30. We further applied a filter on read depth with a minimum of 10-fold and maximum of 600-fold coverage (based on the average coverage estimated for both libraries). The consensus sequences of the Wrangel and Oimyakon individuals were aligned to previously published complete woolly mammoth mitochondrial genomes [S15, S19, S21-S23] (accession numbers: EU155210, DQ188829, EU153446, EU153448, EU153450, EU153451, EU153453, DQ316067, EU153444, EU153445, EU153447, EU153449, EU153452, EU153454 - EU153458), the complete mitochondrial genome of a mastodon (*Mammut americanus*; EF632344) and two modern mitochondrial genomes from an African elephant (*Loxodonta africana*; DQ316069) and an Asian elephant (*Elephas maximus*; DQ316068) using ClustalW [S24] with default parameters built in the software

Geneious [S25] v.5.5.7. Bayesian phylogenies were constructed in BEAST v1.8.0 [S26] for two datasets: *i)* including all woolly mammoth mt genomes together with the mt genomes of the mastodon and the African and Asian elephants and *ii)* including woolly mammoth genomes with finite radiocarbon dates. For dataset (*ii*), which included only intraspecific mt genome sequences, a dated phylogeny was constructed in BEAST using the age of each sequence as tip-date to internally calibrate the molecular clock of the genealogy. Radiocarbon dates from all previously published mt genomes and the two new mt genomes were calibrated in OXCAL [S6] v. 4.2 with the IntCal 13 calibration curve [S7] and their median calibrated dates were used as tip-dates in BEAST. Woolly mammoth mt genome sequences belonging to mtDNA clade I or II were assigned to two groups and the highest posterior density (HPD) of the sequence divergence time between the two clades was estimated based on the inferred rate of molecular evolution. MrModeltest2 [S27] was used to select the best-fitting model of sequence evolution (GTR+I+G for dataset [*i*] and HKY+I+G for a dataset [*ii*]). Analyses were run under a constant-size coalescent tree prior for 50,000,000 iterations sampling every 5,000 generations. Convergence was checked in Tracer [S28] v1.6 with the first 10% of the samples discarded as burn-in.

From the topologies of both phylogenetic trees (Figure S2) we show that the Wrangel individual belonged to mtDNA clade I [S11, S21] (haplogroups C+D+E in [S5]) in agreement with all other specimens from Wrangel Island that have been previously analysed for their mtDNA [S2, S3]. The Oimyakon individual on the other hand, was found to belong to mtDNA clade II [S11, S21] (haplogroup A in [S5]). Using the dates of the mt genomes as internal calibration points in BEAST we dated the coalescence

between the two mtDNA clades at 1.12 million years (MY) with a 95% HPD of 0.36-2.21 MY. This estimate of divergence time is similar to that reported by a previous study that used mt genomes with tip-calibration [S21] (95% HPD: 0.38-2.43 MY). However, both these estimates are much older than the split time reported by another more recent study [S29] (95% credibility interval: 156-261 thousand years ago) that used a larger sample size of dated mtDNA sequences that were 741bp long. This discrepancy could be related to the lack of temporal signal for tip calibration in the complete mt genomes dataset [S30, S31] in contrast to the larger dataset with dated mtDNA sequences [S29]. Sequencing of additional complete mtDNA genomes from a wider temporal range should resolve this issue.

DNA damage analyses

Ancient DNA (aDNA) is characterized by nucleotide misincorporations, in particular C to T and G to A substitutions, which mainly derive from cytosine deamination [S32]. The frequency of these nucleotide misincorporations has been found to be elevated at the 5' end (C to T changes) and 3' end (G to A changes) of the reads sequenced from double-stranded libraries due to single-stranded overhanging ends and nicks in aDNA molecules [S13]. Uracils, the result of cytosine deamination, were removed from both DNA extracts using uracil DNA glycosylases (UDG) in the USER enzyme mix (New England Biolabs) prior to library preparation. In contrast, the pooled libraries in our initial shotgun sequencing experiment were not treated with UDG. We used PMDtools [S33] v.0.53 to assess the damage profiles of our libraries. Figures S1A-B show that the UDG-treated libraries exhibit only a small residual signal of nucleotide misincorporations at the 5' and 3' end of the sequences, whereas the non-treated libraries exhibit significantly higher

nucleotide misincorporation rates towards the terminal positions (Figure S1C). When looking at the damage patterns of the mtDNA, no signal of damage is observed in the UDG-treated Wrangel library (Figure S1D). The slightly elevated but constant rate of nucleotide misincorporations across the mtDNA reads displayed by Oimyakon (Figure S1E) most likely represents real substitutions rather than damage-derived substitutions since Oimyakon is phylogenetically grouped within mtDNA clade II and the mtDNA reference used for alignment belongs to mtDNA clade I (Figure S2).

We restricted the damage analysis to nucleotides in CpG context and noticed as expected that UDG-treatment was less efficient in this case, especially towards the 5' and 3' end of the molecules (misincorporation rate up to 20%; Figures S1F-G). This is due to deaminated methylated cytosines, which result in thymine residues and thus cannot be repaired by UDG-treatment [S13]. Further, the estimated elevated misincorporation rate across the reads (~5%) probably reflects real substitutions given the divergence time between woolly mammoths and African elephant (4.2-9MY) [S34], which was used as a reference, and the fact that the mutation rate in CpG dinucleotides is higher compared to cytosines in a non-CpG context [S35]. We do not observe the same damage pattern when restricting the analysis to nucleotides in a CpG context in the mtDNA (Figures S1H-I), which can be explained by the fact that CpG methylation does not occur in the mtDNA [S13].

Sex identification

The specimen from Wrangel Island consists of a single molar [S1] and thus morphological sex determination was not possible. Similar issues prevented sex

determination of the Oimyakon calf remains due to absence of the posterior body part and genitalia [S4]. In order to determine the sex of these two individuals, we could estimate the ratio of reads aligning to chromosomes X and Y [S36]. However, the absence of an elephant Y-chromosome sequence in the African savanna elephant genome (LoxAfr4) used as reference means that we could not use this method. As an alternative method, we counted the number of reads that mapped against chromosome X (17805622 and 15063126 for Wrangel and Oimyakon, respectively) and compared it to the number of reads that mapped against chromosome 8 (30356668 and 24870030, respectively), which has comparable size to that of chromosome X (~120Mb and ~128Mb respectively). For individuals carrying two X chromosomes, we do not expect to find a significant difference between the proportion of reads mapped against chromosome X and chromosome 8. We normalized by the length of the reference sequences and found that the number of reads that mapped to chromosome X is ~63% = (17805622 /120050768) / (30356668 /128409435) and ~65% = (15063126 /120050768) / (24870030 /128409435) for Wrangel and Oimyakon respectively, of what would be expected based on the chromosome 8 observation. This finding strongly suggests that these two individuals carried only one X chromosome and therefore were both likely to be males.

Genome-wide heterozygosity

We estimated autosomal heterozygosity using mlRho's v.2.7 [S37] population mutation rate (θ) estimate, which approximates expected heterozygosity under the infinite sites model. We filtered out bases with quality below 30, reads with mapping quality below 30 and positions with root-mean-squared mapping quality below 30. High or low coverage in some regions can result from structural variation that can create erroneous mapping to

the reference genome leading to observed false heterozygous sites. In order to avoid this problem, we applied a filter on coverage excluding sites with depth lower than 1/3 and higher than 2 times the estimated average coverage for each library. The maximum likelihood approach implemented in mlRho has been shown to provide unbiased estimates of average within-individual heterozygosity at high coverage [S37, 38]. Therefore, we did not correct for the lower coverage of the Oimyakon genome, 11.2-fold versus the 17.1-fold coverage of the Wrangel genome, in our comparison of autosomal heterozygosity between the two individuals. The estimates from mlRho reveal lower levels of autosomal heterozygosity for the Wrangel individual than the Oimyakon individual (Table S2) despite coverage discrepancies.

We also calculated heterozygosity in chromosome X using mlRho with the same filters as described above for the autosomes. Since chromosome X is in haploid state in males, we did not expect to find any heterozygous sites (excluding sequencing errors and remaining damage-derived misincorporations on CpG sites) in the chrX sequence of the two individuals assumed to be males. The estimated number of heterozygous sites was 4.39 (confidence interval [CI]: 2.72-6.61) and 2.25 (CI: 0.88-4.57) per 10,000bp in the X chromosome of the Wrangel and Oimyakon individual respectively (Table S2). These estimates are lower than the respective autosomal heterozygosity estimates and at the same order of magnitude but not lower than the estimated sequencing error in chromosome X. To look into this further, we assessed whether heterozygosity estimates varied across chromosome X by calculating regional heterozygosity per 10kb windows. We called a consensus sequence for chromosome X using SAMtool's [S18] (version 0.1.19) 'mpileup' command and the 'vcf2fq' command from vcfutils.pl filtering out bases

with the same quality and coverage filters as described above. We then used seqtk's (https://github.com/lh3/seqtk) 'comp' tool to estimate the number or heterozygous sites per 10kb non-overlapping windows and found that certain regions of chromosome X contain higher numbers of heterozygous sites compared to the rest of the chromosome in both individuals, especially at the beginning and end of chromosome X. Interestingly, the positions of high-heterozygosity regions observed on the Wrangel chromosome X match with those on the Oimyakon chromosome X. We suspect that regions of high heterozygosity correspond to recombining regions (known as pseudo-autosomal regions (PAR) and non-recombining homologous regions between chromosomes X and Y [S39]. We therefore conclude that the estimated average heterozygosity across chromosome X is elevated due to the inclusion of heterozygous sites between chromosome X and Y at homologous regions. Remaining heterozygous sites distributed across the X chromosome most likely represent sequencing errors and remaining damage-derived misincorporations on CpG sites.

Genetic divergence between the two mammoths and the African savanna elephant

We estimated the sequence divergence between the Oimyakon and Wrangel individuals as well as between each one of them and the African savanna elephant reference genome. We called sequences for all autosomes using a majority calling rule that required at least 3-fold coverage at each position. This approach was used to alleviate potential biases from differences in coverage between the two samples. We computed the probability that the two mammoth sequences were different per base pair and the probability that each mammoth sequence was different from the African savanna elephant sequence per base pair using *i)* all substitutions, *ii)* only tranversions to exclude CpG sites with post-mortem

damage. Based on this method, we detect 3,520,698 high-quality SNPs between the Wrangel and Oimyakon genomes. Using all substitutions, we find that the divergence of the Wrangel and Oimyakon individuals to the African elephant reference genome is 0.74%, and 0.71% respectively, similar to previous divergence estimates from low-coverage genome-wide data [S40]. Using only transversions, these estimates correspond to 0.22% and 0.21% respectively. The sequence divergence between the Wrangel individual and the Oimyakon individual is 0.16%, similar to the heterozygosity observed in the Oimyakon individual (Table S2; 0.05% when using only transversions).

Using the genetic divergence between the Wrangel mammoth and the African savanna elephant estimated above (0.74%) and assuming a genome-wide average genetic divergence time between African and Eurasian elephants $T_{\text{div(African-Eurasian)}}$, we can estimate the substitution rate. Rohland et al. [S34] estimated the relative population split time between African and Eurasian elephants ($\tau_{\text{Afr-Eur}} = T_{\text{Afr-Eur}}\mu$) and relative effective population size of their ancestral population ($\theta_{\text{Afr-Eur}} = 4N_{\text{Afr-Eur}}\mu g$) in terms of coalescent units, where $T_{\text{Afr-Eur}}$ is the population split time in years, μ is the mutation rate per year, $N_{\text{Afr-Eur}}$ is the effective population size in individuals and g is the generation time in years. We used these relative estimates to calculate the ratio of genetic divergence time divided by the population split time $T_{\text{div(Afr-Eur)}}/T_{\text{Afr-Eur}} = 1+(\theta_{\text{Afr-Eur}}/2\tau_{\text{Afr-Eur}})$. Specifically, we used the 90% confidence intervals of these parameters to take into account the uncertainty in their estimate and derived a ratio equal to 1.48 – 1.93. Assuming a population split time $T_{\text{Afr-Eur}}$ = 4.2 – 9 million years (based on the paleontological record as justified in [S34]) the genetic divergence time is equal to 6.2 – 17.4 MY. Using this time range to calibrate the molecular clock, we obtain a range of substitution rates equal to 0.21×10^{-9} – 0.6×10^{-9}

per bp per year (Table 1). This paleontological calibration was used as a more conservative approach for the subsequent inferences of demographic parameters, along with the novel PSMC-based substitution rate and its range of uncertainty estimated in this study (described in detail in the following section).

PSMC and population split time analyses

Inference of population size changes over time

We used the Pairwise Sequential Markovian Coalescent (PSMC) model [S41] to reconstruct the population history of each woolly mammoth individual. This method implements a hidden Markov Model to infer changes in the density of heterozygous sites across the diploid genome of a single individual. Regions of low heterozygosity reflect recent coalescent events while regions of high heterozygosity reflect more ancient coalescent events. The rate of coalescent events in each segment is then informative about changes in effective population size through time since the rate of coalescence is inversely proportional to effective population size. Consensus sequences were generated for all autosomes of both genomes using SAMtool's [S18] (version 0.1.19) 'mpileup' command and the 'vcf2fq' command from vcfutils.pl. Filters for base quality, mapping quality and root-mean-squared mapping quality below 30, and depth below 1/3 and higher than 2-times the average coverage estimated for each library were applied. The PSMC method was used with default parameters (64 atomic time intervals: 4+25*2+4+6, for each of which parameters are estimated with 28 free interval parameters) to infer the distribution of the time to the most recent common ancestor (TMRCA) between the two copies of each chromosome from each individual across all autosomes. Bootstrapping

was performed by splitting long chromosomes to short segments using default parameters and PSMC was run 100 times by sampling with replacement from those segments. The inference of effective population size (N_e) changes across time from the original PSMC analysis and each bootstrap analysis was then plotted for each genome (Figure S3A). The PSMC curves for the Wrangel and Oimyakon genomes appear to capture a similar, at least qualitatively, population history until their recent past. The inferred history includes a considerable decrease in N_e at some time in the past followed by population recovery. Subsequently, the Oimyakon population size seems to have remained relatively stable over time, with only minor changes in N_e. On the other hand, the Wrangel population crashes rather suddenly to significantly low N_e after a time period of relative stability.

Substitution rate estimation using the PSMC curves

The PSMC curves from diploid genomes of dated individuals with considerably different ages that are assumed to have originated from the same ancestral population can be used to scale time on the x-axis from divergence units to years. From this scaling, we can derive the substitution rate. Both the Wrangel and Oimyakon individuals have finite radiocarbon dates with an age difference of 40,500 years. Moreover, the inferred population size over time estimated by the PSMC of the Wrangel genome is similar to that of the Oimyakon genome (excluding the recent past; Figure S3A). We plotted the PSMC curves of both genomes simultaneously and gradually shifted the Oimyakon curve away from the origin across the x-axis until both curves lined up. The divergence (d) estimated from the shift of the Oimyakon curve on the x-axis should be equal to $2\mu(\Delta T)$, where ΔT is the age difference of the two genomes in generations and μ the population substitution rate. Figure S3C shows that the Oimyakon curve was shifted to the right

along the x-axis until the two curves roughly lined up for $\mu = 10^{-4}$ (range = 4×10^{-5} – 1.5×10^{-4}). It should be noted that because the coverage of the Oimyakon genome is lower than that of the Wrangel genome (11.2-fold versus 17.1-fold), we applied a correction for missing heterozygotes [S41] that was empirically estimated (false negatives [FN] = 30%) when plotting the PSMC curve for the Oimyakon genome. Using this method we obtained an estimate of 1.23×10^{-9} substitutions per nucleotide per year (range = 0.49×10^{-9} – 1.85×10^{-9}), which is equivalent to 3.83×10^{-8} substitutions per nucleotide per generation (range = 1.53×10^{-8} – 5.73×10^{-8}) assuming 31 years per generation [S34].

Assuming the substitution rate estimated above and generation time = 31 years [S34], we rescaled N_e on the y-axis of the PSMC curves to investigate the effective population size at different stages of the woolly mammoth's history. During the earlier bottleneck, N_e is estimated to have dropped to ~3,000 individuals (approximate range based on the range of uncertainty from the PSMC-based and paleontological calibration: 2,000 - 19,000 individuals; Table 1) whereas maximum N_e after recovery reached ~13,000 individuals (approximate range: 9,000 – 76,000 individuals; Table 1). The effective population size on Wrangel Island following the bottleneck is estimated at 328 individuals (218 – 823 individuals based on the PSMC-inferred range of substitution rates). This is lower than earlier inferences of N_e from microsatellite data (posterior 95% CI: 1,000-8,300) [S42] but within the range of the estimated carrying capacity of the island (149-819 individuals) [S2]. Assuming the paleontological calibration, the N_e on Wrangel Island following the bottleneck is estimated at 676 – 1,896 individuals (Table 1), a range which appears to be too high given the estimated carrying capacity of the island. The relatively large N_e predating the earlier bottleneck reflects a few coalescent events per time unit compared to

the time periods before and after. This feature could be interpreted as a true increase in effective population size or could be explained by population structure involving separation and admixture, which would inflate estimates of effective population size. The latter scenario could be possible given that primitive woolly mammoth morphology first appears in the fossil record at about 700,000 years ago, replacing its predecessor *Mammuthus trogontherii* [S43].

Testing for Inbreeding

We plotted the inferred time to the most recent common ancestor (TMRCA) at every position of the genome from the posterior decoding of the PSMC [S20, S41]. Regions with low levels of heterozygosity (runs of homozygosity) reflect recent common ancestry while regions with high numbers of heterozygous sites reflect more ancient ancestry. More, as well as longer, regions of low heterozygosity were detected on the Wrangel genome compared to the Oimyakon genome (Figures 3B-C), indicating that the Wrangel individual shares common ancestors within the last dozens of generations. Figure S4 illustrates the distribution of the TMRCA across all autosomes with the longest stretch of recent ancestry extending ~13Mb along chromosome 1 in the Wrangel genome. Overall, 23.3% of the Wrangel genome was inferred to have coalesced in the most recent bin in contrast to 0.83% of the Oimyakon genome.

Population split time

Since both individuals were predicted to be males (see sex identification section for more details), their X chromosome sequences are naturally phased and can therefore be combined to build a pseudo-diploid genome. Because the PSMC infers the TMRCA

between two alleles carried by one individual across its genome, this method can be used in a similar way to infer the TMRCA between two haploid genomes from two populations [S41]. The inferred population size history of the pseudo-diploid genome can then be studied to investigate the relationships of the two populations. The inferred N_e parameter is inversely proportional to the rate of coalescences between the two chromosomes, and thus we expect inferred N_e to be very large for periods where the ancestral populations were isolated from each other. We extracted the X chromosome consensus sequences of the Wrangel and Oimyakon individuals as described in the genome-wide heterozygosity section. We then merged the two haploid X chromosome sequences into a pseudo-diploid sequence, suppressing heterozygous sites that were called in each consensus and masking the first 10MB at the beginning of the chromosome to exclude the recombining PAR region. Sites that differed between the two consensus sequences were marked as "heterozygous" in the pseudo-diploid chromosome X. We applied the PSMC method on the pseudo-diploid chromosome X to estimate changes in the N_e parameter over time. Originally, default parameters of the PSMC model (64 discrete intervals: 4+25*2+4+6; as described above for the autosomes) were used. However, we found that the number of free interval parameters (1+25+1+1) led to overfitting and we thus decided to reduce them by using 49 discrete intervals (6+4+3+13*2+4+6). We also performed a bootstrap analysis by splitting the pseudo-diploid chromosome X to short segments using 5MB segments and PSMC was run 100 times by sampling with replacement from those segments (Figure S3B).

Figure 1C shows the PSMC output from the pseudo-diploid chromosome X compared to the Wrangel genome and Oimyakon genome. The PSMC curve of the pseudo-diploid X

chromosome was scaled to 0.75 as expected for the effective population size of chromosome X relative to that of autosomes, assuming no sex differences in dispersal and variance of reproductive success. In elephants, these factors are known to be sex-biased, where most females have high reproductive success and do not disperse while males disperse but very few are successful at mating [S44-S47]. Although sex-biased dispersal and reproductive success could affect the X-chromosome:autosome N_e ratio so that it deviates from 0.75 [S34, S48], the use of an alternative N_e ratio would shift the pseudo-diploid X-chromosome PSMC curve along the y-axis and therefore not affect its time scale and subsequent inference of population split time. The PSMC curve of the pseudo-diploid chromosome X was also empirically corrected for missing heterozygotes (FN = 30%) and shifted away from the origin on the x-axis so that it ends at ~24,500 years ago, the average age of the two individuals. This time point was scaled in divergence units based on the substitution rate estimated in this section. If we exclude the very recent and ancient past, where PSMC has lower power for inference due to few coalescent events and errors from segmental duplications respectively [S41], we notice that the population history of the pseudo-diploid chromosome X agrees well with the histories inferred from the two diploid genomes. The PSMC curve of chromosome X deviates from the other two curves just before the time of the death of the Oimyakon individual, indicating population separation. Inferred N_e reaches nearly infinity at this point since no more coalescent events can happen after the death of the Oimyakon individual (~45,000 years BP), suggesting no or little genetic differentiation between the two populations. To investigate this further we used an extension of the PSMC method on the pseudo-diploid X chromosome that estimates the split time (T), assuming no

coalescent events since divergence [S49]. To avoid underestimation of the split time, we used fewer discrete intervals (20+4*5). The inferred split time scaled in $2\mu T$ was estimated at 6.2×10^{-5}. Assuming the substitution rate estimated in this section, the split time corresponds to ~50,000 (= 25,295 + 24,582 years, the average age of the two individuals). The estimated range of split times taking into account the uncertainty in the PSMC-based inference of substitution rates and the paleontological calibrations corresponds to 41,000 – 171,000 years, again indicating a very recent split for the two populations (Table 1).

In addition to the X-chromosome-based population divergence time estimation, we investigated an independent approach based on discovering heterozygous sites in an individual B and estimating the probability $F(A|B)$ that a second individual A carries the derived allele at a single randomly chosen chromosome [S50]. This is based on the rationale that when two populations diverge, they start to accumulate mutations that will not, assuming complete isolation, be present in other populations.

We ascertained heterozygote positions in the Oimyakon individual that passed our quality filters (base and mapping quality above 30, genotype quality above 40, filtering out sites that surrounded an indel [-5bp/+5bp]), and estimated the probability that a randomly sampled chromosome from the Wrangel individual would carry the derived allele, which was polarized using the African elephant genome. We found 633,613 such informative sites after excluding all transitions, and computed a standard error for $F(A|B)$ using a weighted block jackknife over 516 contiguous blocks of 5Mb. We estimate F(Wrangel | Oimyakon) = 32.95 ± 0.14%, which is close to the theoretical expectation of 1/3 if A and B are from a single constant size population. When transitions are included, we estimate a

very similar $F = 33.26\% \pm 0.13\%$ from a total of 2,063,264 informative sites. We focus on transversions here both to avoid lingering effects of post-mortem damage in CpG context, and also since transversions have a slower mutation process, and are thus less likely to be affected by homoplasies in the elephant genome.

Randomly sampling a single gene copy effectively makes population size fluctuations in the population of individual A irrelevant to the inference, and we are left with accounting for genetic drift in the lineage leading to individual B. To calibrate the F-statistic to the population size history of Oimyakon, we simulated the population size trajectory inferred using PSMC, for 100 regions each of 30Mb. Finding the intersection between the empirical value and the expected decay of $F(A|B)$ as a function of split time, we find that Oimyakon diverged from the population lineage leading to Wrangel at most $t = 0.055$ time units (measured in N_0 generations, where N_0 is the terminal population size) prior to the death of the Oimyakon individual (Figure 2). This time falls in the second PSMC interval of Oimyakon's history, which corresponds well to the inferred time of cessation of coalescences between the X-chromosomes of Wrangel and Oimyakon. Assuming the substitution rate estimated in this section, the population split time is approximately 8,000 – 19,000 years prior to the death of the Oimyakon mammoth, which corresponds to 53,000 – 64,000 years ago. The obtained range of split times using the PSMC-inferred range of substitution rates and the paleontological calibrations is equal to 5,000 – 48,000 years and 17,000 – 110,000 years prior to the death of the Oimyakon mammoth, respectively (Table 1).

Supplemental References

1. Vartanyan, S.L., Arslanov, K.A., Karhu, J.A., Possnert, G., and Sulerzhitsky, L.D. (2008). Collection of radiocarbon dates on the mammoths (*Mammuthus primigenius*) and other genera of Wrangel Island, northeast Siberia, Russia. Quaternary Research *70*, 51.
2. Nyström, V., Dalén, L., Vartanyan, S., Lidén, K., Ryman, N., and Angerbjörn, A. (2010). Temporal genetic change in the last remaining population of woolly mammoth. Proceedings Of The Royal Society B-Biological Sciences *277*, 2331-2337.
3. Nyström, V., Humphrey, J., Skoglund, P., McKeown, N.J., Vartanyan, S., Shaw, P.W., Lidén, K., Jakobsson, M., Barnes, I., Angerbjörn, A., et al. (2012). Microsatellite genotyping reveals end-Pleistocene decline in mammoth autosomal genetic variation. Molecular Ecology *21*, 3391-3402.
4. Maschenko, E.N., Boeskorov, G.G., and Baranov, V.A. (2013). Morphology of a mammoth calf (Mammuthus primigenius) from Ol'chan (Oimiakon, Yakutia). Paleontol. J. *47*, 425-438.
5. Debruyne, R., Chu, G., King, C.E., Bos, K., Kuch, M., Schwarz, C., Szpak, P., Gröcke, D.R., Matheus, P., Zazula, G., et al. (2008). Out of America: ancient DNA evidence for a New World origin of Late Quaternary woolly mammoths. Current Biology *18*, 1320.
6. Ramsey, C.B. (2009). Bayesian Analysis of Radiocarbon Dates.

7. Reimer, P.J., Bard, E., Bayliss, A., Beck, J.W., Blackwell, P.G., Bronk Ramsey, C., Buck, C.E., Cheng, H., Edwards, R.L., Friedrich, M., et al. (2013). IntCal13 and Marine13 Radiocarbon Age Calibration Curves 0–50,000 Years cal BP.

8. Yang, D.Y., Eng, B., Waye, J.S., Dudar, J.C., and Saunders, S.R. (1998). Improved DNA extraction from ancient bones using silica-based spin columns. American Journal of Physical Anthropology *105*, 539-543.

9. Brace, S., Palkopoulou, E., Dalén, L., Lister, A.M., Miller, R., Otte, M., Germonpré, M., Blockley, S.P.E., Stewart, J.R., and Barnes, I. (2012). Serial population extinctions in a small mammal indicate Late Pleistocene ecosystem instability. Proceedings of the National Academy of Sciences *109*, 20532-20536.

10. Rohland, N., and Hofreiter, M. (2007). Comparison and optimization of ancient DNA extraction. Biotechniques *42*, 343-352.

11. Barnes, I., Shapiro, B., Lister, A., Kuznetsova, T., Sher, A., Guthrie, D., and Thomas, M.G. (2007). Genetic structure and extinction of the woolly mammoth, *Mammuthus primigenius*. Current Biology *17*, 1072.

12. Meyer, M., and Kircher, M. (2010). Illumina Sequencing Library Preparation for Highly Multiplexed Target Capture and Sequencing. Cold Spring Harbor Protocols *2010*, pdb.prot5448.

13. Briggs, A.W., Stenzel, U., Meyer, M., Krause, J., Kircher, M., and Pääbo, S. (2010). Removal of deaminated cytosines and detection of in vivo methylation in ancient DNA. Nucleic Acids Research *38*, e87.

14. Kircher, M., Sawyer, S., and Meyer, M. (2012). Double indexing overcomes inaccuracies in multiplex sequencing on the Illumina platform. Nucleic Acids Research *40*, e3.

15. Poinar, H.N., Schwarz, C., Qi, J., Shapiro, B., MacPhee, R.D.E., Buigues, B., Tikhonov, A., Huson, D.H., Tomsho, L.P., Auch, A., et al. (2006). Metagenomics to paleogenomics: Large-scale sequencing of mammoth DNA. Science *311*, 392-394.

16. Quail, M.A., Kozarewa, I., Smith, F., Scally, A., Stephens, P.J., Durbin, R., Swerdlow, H., and Turner, D.J. (2008). A large genome center's improvements to the Illumina sequencing system. Nat Meth *5*, 1005-1010.

17. Li, H., and Durbin, R. (2009). Fast and accurate short read alignment with Burrows–Wheeler transform. Bioinformatics *25*, 1754-1760.

18. Li, H., Handsaker, B., Wysoker, A., Fennell, T., Ruan, J., Homer, N., Marth, G., Abecasis, G., Durbin, R., and Subgroup, G.P.D.P. (2009). The Sequence Alignment/Map format and SAMtools. Bioinformatics *25*, 2078-2079.

19. Krause, J., Dear, P.H., Pollack, J.L., Slatkin, M., Spriggs, H., Barnes, I., Lister, A.M., Ebersberger, I., Paabo, S., and Hofreiter, M. (2006). Multiplex amplification of the mammoth mitochondrial genome and the evolution of Elephantidae. Nature *439*, 724-727.

20. Prufer, K., Racimo, F., Patterson, N., Jay, F., Sankararaman, S., Sawyer, S., Heinze, A., Renaud, G., Sudmant, P.H., de Filippo, C., et al. (2014). The complete genome sequence of a Neanderthal from the Altai Mountains. Nature *505*, 43-49.

21. Gilbert, M.T.P., Drautz, D.I., Lesk, A.M., Ho, S.Y.W., Qi, J., Ratan, A., Hsu, C.H., Sher, A., Dalén, L., Götherström, A., et al. (2008). Intraspecific phylogenetic analysis of Siberian woolly mammoths using complete mitochondrial genomes. Proceedings Of The National Academy Of Sciences Of The United States Of America *105*, 8327-8332.

22. Rogaev, E.I., Moliaka, Y.K., Malyarchuk, B.A., Kondrashov, F.A., Derenko, M.V., Chumakov, I., and Grigorenko, A.P. (2006). Complete mitochondrial genome and phylogeny of Pleistocene mammoth Mammuthus primigenius. Plos Biology *4*, 403-410.

23. Gilbert, M.T.P., Tomsho, L.P., Rendulic, S., Packard, M., Drautz, D.I., Sher, A., Tikhonov, A., Dalén, L., Kuznetsova, T., Kosintsev, P., et al. (2007). Whole-genome shotgun sequencing of mitochondria from ancient hair shafts. Science *317*, 1927-1930.

24. Larkin, M.A., Blackshields, G., Brown, N.P., Chenna, R., McGettigan, P.A., McWilliam, H., Valentin, F., Wallace, I.M., Wilm, A., Lopez, R., et al. (2007). Clustal W and Clustal X version 2.0. Bioinformatics *23*, 2947-2948.

25. Geneious version 5.5.7 created by Biomatters. Available from http://www.geneious.com/

26. Drummond, A.J., Suchard, M.A., Xie, D., and Rambaut, A. (2012). Bayesian Phylogenetics with BEAUti and the BEAST 1.7. Molecular Biology and Evolution *29*, 1969-1973.

27. Nylander, J.A.A. (2004). MrModeltest v2. (Program distributed by the author. Evolutionary Biology Centre, Uppsala University).

28. Rambaut, A., Suchard, M., Xie, D., and Drummond, A. (2014). Tracer v1.6. Available from http://beast.bio.ed.ac.uk/Tracer.

29. Palkopoulou, E., Dalén, L., Lister, A.M., Vartanyan, S., Sablin, M., Sher, A., Edmark, V.N., Brandström, M.D., Germonpré, M., Barnes, I., et al. (2013). Holarctic genetic structure and range dynamics in the woolly mammoth. Proceedings of the Royal Society B: Biological Sciences *280*.

30. Drummond, A.J., Pybus, O.G., Rambaut, A., Forsberg, R., and Rodrigo, A.G. (2003). Measurably evolving populations. Trends in Ecology & Evolution *18*, 481-488.

31. Ho, S.Y.W., Lanfear, R., Phillips, M.J., Barnes, I., Thomas, J.A., Kolokotronis, S.-O., and Shapiro, B. (2011). Bayesian Estimation of Substitution Rates from Ancient DNA Sequences with Low Information Content. Systematic Biology *60*, 366-375.

32. Briggs, A.W., Stenzel, U., Johnson, P.L.F., Green, R.E., Kelso, J., PrÃ¼fer, K., Meyer, M., Krause, J., Ronan, M.T., Lachmann, M., et al. (2007). Patterns of damage in genomic DNA sequences from a Neandertal. Proceedings of the National Academy of Sciences *104*, 14616-14621.

33. Skoglund, P., Northoff, B.H., Shunkov, M.V., Derevianko, A.P., Pääbo, S., Krause, J., and Jakobsson, M. (2014). Separating endogenous ancient DNA from modern day contamination in a Siberian Neandertal. Proceedings of the National Academy of Sciences *111*, 2229-2234.

34. Rohland, N., Reich, D., Mallick, S., Meyer, M., Green, R.E., Georgiadis, N.J., Roca, A.L., and Hofreiter, M. (2010). Genomic DNA Sequences from Mastodon

and Woolly Mammoth Reveal Deep Speciation of Forest and Savanna Elephants. PLoS Biol *8*, e1000564.

35. Sved, J., and Bird, A. (1990). The expected equilibrium of the CpG dinucleotide in vertebrate genomes under a mutation model. Proceedings of the National Academy of Sciences *87*, 4692-4696.

36. Skoglund, P., Storå, J., Götherström, A., and Jakobsson, M. (2013). Accurate sex identification of ancient human remains using DNA shotgun sequencing. Journal of Archaeological Science *40*, 4477-4482.

37. Haubold, B., Pfaffelhuber, P., and Lynch, M. (2010). mlRho – a program for estimating the population mutation and recombination rates from shotgun-sequenced diploid genomes. Molecular Ecology *19*, 277-284.

38. Lynch, M. (2008). Estimation of Nucleotide Diversity, Disequilibrium Coefficients, and Mutation Rates from High-Coverage Genome-Sequencing Projects. Molecular Biology and Evolution *25*, 2409-2419.

39. El-Mogharbel, Nisrine, and Graves, and Jennifer, A. (2008). X and Y Chromosomes: Homologous Regions. eLS *doi: 10.1002/9780470015902.a0005793.pub2*.

40. Miller, W., Drautz, D.I., Ratan, A., Pusey, B., Qi, J., Lesk, A.M., Tomsho, L.P., Packard, M.D., Zhao, F., Sher, A., et al. (2008). Sequencing the nuclear genome of the extinct woolly mammoth. Nature *456*, 387-390.

41. Li, H., and Durbin, R. (2011). Inference of human population history from individual whole-genome sequences. Nature *475*, 493-496.

42. Skoglund, P., Sjödin, P., Skoglund, T., Lascoux, M., and Jakobsson, M. (2014). Investigating Population History Using Temporal Genetic Differentiation. Molecular Biology and Evolution *31*, 2516-2527.

43. Lister, A.M., Sher, A.V., van Essen, H., and Wei, G.B. (2005). The pattern and process of mammoth evolution in Eurasia. Quaternary International *126-28*, 49-64.

44. Hollister-Smith, J.A., Poole, J.H., Archie, E.A., Vance, E.A., Georgiadis, N.J., Moss, C.J., and Alberts, S.C. (2007). Age, musth and paternity success in wild male African elephants, Loxodonta africana. Animal Behaviour *74*, 287-296.

45. Rasmussen, H.B., Okello, J.B.A., Wittemyer, G., Siegismund, H.R., Arctander, P., Vollrath, F., and Douglas-Hamilton, I. (2008). Age- and tactic-related paternity success in male African elephants. Behavioral Ecology *19*, 9-15.

46. Ishida, Y., Oleksyk, T.K., Georgiadis, N.J., David, V.A., Zhao, K., Stephens, R.M., Kolokotronis, S.-O., and Roca, A.L. (2011). Reconciling Apparent Conflicts between Mitochondrial and Nuclear Phylogenies in African Elephants. PLoS ONE *6*, e20642.

47. Brandt, A.L., Ishida, Y., Georgiadis, N.J., and Roca, A.L. (2012). Forest elephant mitochondrial genomes reveal that elephantid diversification in Africa tracked climate transitions. Molecular Ecology *21*, 1175-1189.

48. Hedrick, P.W., and Rausher, M. (2007). SEX: DIFFERENCES IN MUTATION, RECOMBINATION, SELECTION, GENE FLOW, AND GENETIC DRIFT. Evolution *61*, 2750-2771.

49. Prado-Martinez, J., Sudmant, P.H., Kidd, J.M., Li, H., Kelley, J.L., Lorente-Galdos, B., Veeramah, K.R., Woerner, A.E., O/'Connor, T.D., Santpere, G., et al. (2013). Great ape genetic diversity and population history. Nature *499*, 471-475.

50. Green, R.E., Krause, J., Briggs, A.W., Maricic, T., Stenzel, U., Kircher, M., Patterson, N., Li, H., Zhai, W.W., Fritz, M.H.Y., et al. (2010). A Draft Sequence of the Neandertal Genome. Science *328*, 710-722.